ANALYSIS OF PULSATILE FLOW IN ARTERIOVENOUS FISTULA THROUGH NUMERICAL SIMULATION

Willyam Brito de Almeida Santos, Universidade Federal do Rio Grande do Norte, willyambas@gmail.com
Jonhattan Ferreira Rangel, Universidade Federal do Rio Grande do Norte, jferreirarangel01@gmail.com
Valquíria Bomfim Fernandes, Universidade Federal do Rio Grande do Norte, valbfernandes@gmail.com
Luiz Henrique Pinheiro de Lima, Universidade Federal do Rio Grande do Norte, henriqueengmec@yahoo.com.br
Thércio Henrique de Carvalho Costa, Universidade Federal do Rio Grande do Norte, thercioc@hotmail.com
Kleiber Lima de Bessa, Universidade Federal do Rio Grande do Norte, klbessa@ct.ufrn.br

Abstract. *This work aim to analyze the hemodynamic factors in the flow within an Arteriovenous Fistula (AVF) using a flow field calculated by numerical simulation as a visualization technique. The geometrical model is virtually reconstructed from a computed tomography scan. The considerations made are of Newtonian fluid, laminar and incompressible flow and pulsatile flow. Primary and secondary flows are observed in the velocity field along the AVF. In the artery, the velocity profile is typical of a laminar flow. In the anastomosis and distal regions, axial and radial recirculations are observed. The maximum velocity calculated along the AVF is 1.38 m/s. The maximum wall shear stress is of 49 Pa and shows no uniformity, varying according to velocity. The presence of recirculations allows blood formed elements to collide excessively against the endothelial wall. At regions with wall shear stress above 35 Pa, the endothelial cells can suffer damage and myointimal hyperplasia may form.*

Key words*: Arteriovenous fistula. Shear stress. Numerical simulation. Intimal hyperplasia.*

1. INTRODUCTION

The Arteriovenous Fistula (AVF) is the main technique used for vascular access during hemodialysis treatment for kidney diseases. This method is used to ensure adequate blood flow during the hemodialysis session and it presents the best results in terms of vascular access, lower morbidity and mortality rates when compared to individuals who utilize central venous catheters or grafts. Furthermore, the AVF has overall low costs (Gill *et al.*, 2016) (Lok, 2016). Linardi *et al.* (2003) studied 23 units of Brazilian dialysis units and concluded that the majority of patients who submit to a vascular access for hemodialysis do so via AVF. Despite being the most commonly used technique, certain clinical factors render its functionality impossible, such as old age, coronary artery disease and peripheral vascular disease. These factors are associated with fistulas failing to mature, due to diseased vasculature, presenting defects which pose difficulties to the adequate inlet and outlet of blood flow necessary for the process of maturation of the AVF (Lok, 2016).

A common issue to occur in the AVF is intimal hyperplasia (IH). Bassiouny *et al.* (1992) investigated IH in the region of the anastomosis and stated that it relates to biomechanical and hemodynamic factors. They showed the existence of a complex secondary flow pattern in the vicinity of the anastomosis, which can interact with other biomechanical and humoral factors to modulate the exaggerated adaptive response in the scarring of the lesioned arteries. Despite the mechanisms for HI not yet being clear, it is accepted that the local blood flow patterns influence the progression of HI in the anastomosis region.

Other correlations were made in the anastomosis region according to Giddens *et al.* (1990), with the characteristics of flow separation, recirculation, increased residence time of the particles and unstable distribution of shear stress in the endothelium. It was shown that, in the regions where the flow movement was more complex, the magnitudes of the shear stress were increased.

The shear stress exerted on the vessel wall or, more specifically, on the endothelial cells has a crucial role in the development of IH and, according to Bessa and Ortiz (2009), the regions of low wall shear stress are important in the development of vascular diseases, with a marked increase in the formation of atherosclerosis. Rubanyi (1993) showed that the shear stress is one of the stimuli which act upon the endothelial cells, promoting the synthesis of vasodilating or vasoconstricting substances. The balance of these substances is essential for the endothelial cells' ability to maintain the regulatory action of the cardiovascular system. Otherwise, endothelial dysfunction is the fundamental step towards the progression of atherosclerosis (Perraul *et al.*, 2000). Carrol *et al.*, (2009, 2011) showed that IH develops in regions with increased shear stresses, promoting the endothelial denudation and leaving a thrombogenic surface exposed.

This work seeks to contribute to the study of the correlations between the hemodynamic factors in the blood flow within an AVF and complications on the arterial wall. In order to accomplish this, three-dimensional calculations were applied by means of Computational Fluid Dynamics (CFD), as a means of visualization for locating the flow patterns associated with pathologies such as intimal hyperplasia.

2. METHOD

2.1 Geometrical Model and Computational Mesh of the AVF

The three-dimensional geometrical model was obtained by means of computed tomography (CT) scan of a patient with an AVF, provided by the Onofre Lopes University Hospital, of the Federal University of Rio Grande do Norte. The model was virtually reconstructed using the *InVesalius* 3.1.1 software, as seen in Fig. (1a) and received image treatment through the *Autodesk Meshmixer* software, as seen in Fig. (1b).

After an initial surface correction of the AVF through *Meshmixer*, this geometry was exported to the *ANSYS® ICEM CFD™* software, with which three unstructured computational meshes were generated, composed of 620 thousand, 900 thousand and 1 million elements respectively. The increase in the number of elements between meshes was due to refinement at the regions of greater interest, near the vessel wall, in order to observe, in detail the wall shear stress distribution along the AVF. By varying the generated meshes, it was possible to ensure the independence of the resulting data, which showed a difference of 0.6% between meshes. See Fig. (1c).

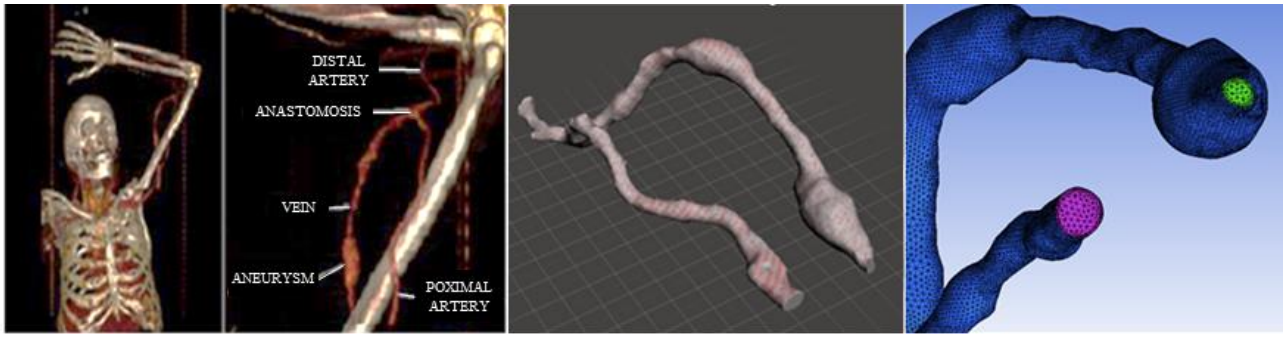

Figure 1. (a) Images obtained via CT scan being processed through *Invesalius*; (b) Images being treated on *Autodesk Meshmixer*; (c) Mesh generated on *ICEM*.

2.2 Numerical Model and Flow Conditions of the AVF

For flow modeling and determining the detailed behavior of the flow field along the AVF, the continuity equation was applied, see Eq. (1), assuming incompressible flow, as well as the momentum equation, see Eq. (2), for transient flow.

$$\nabla \cdot \vec{V} = 0 \tag{1}$$

$$\rho\left(\frac{D\vec{V}}{Dt}\right) = -\nabla p + \mu\nabla^2\vec{V} \tag{2}$$

In these equations, $\vec{V}$ is the three-dimensional velocity vector, t the time, p the pressure, ρ the density and μ absolute viscosity.

The numerical solution was calculated using *ANSYS®Fluent®* software. Blood was defined as the working fluid, with a density of 1050 kg/m³ (Berger *et al.*, 1996). Although blood viscosity is dependent upon shear rate, the blood was considered a Newtonian fluid, since according to Berger *et al.* (1996) viscosity remains constant at approximately 3.003 mPa·s for shear rates greater than 100 s^{-1}, which is lower than the mean strain rate found in arteries.

It was considered in the walls that represent the artery and the vein a non-slip condition imposed on the vectors velocities. The flow was considered transient, with mass flow rate varying over time. The data for mass flow rate at surface 1 and surface 2 was established according to Sigovan *et al.* (2012). The values for the pulse of the mass flow rate were extracted using the *GraphData* software, after which an approximation of the function was obtained by means of Fourier series, using the *Scilab* software, see Fig. (2a). The function was implemented as a *user-defined-function* (UDF) on *ANSYS®Fluent®* software, which established the initial inlet boundary conditions for each time step. SIMPLE was used as an algorithm for pressure-velocity and for surface 3 gauge pressure is set to zero. The simulations presented here are representative of a cyclical phenomenon in time, so they were performed in several cycles, with pulse independence guaranteed with variations in the calculations of 0.8% at maximum between cycles.

Planes of analysis were defined, shown in Fig. (2b): in the artery, (a) the proximal plane; in the vein, (b) the distal 1, (c) distal 2, (d) distal 3 and (e) distal 4 planes; and (f) the anastomosis, connection between the artery and the vein.

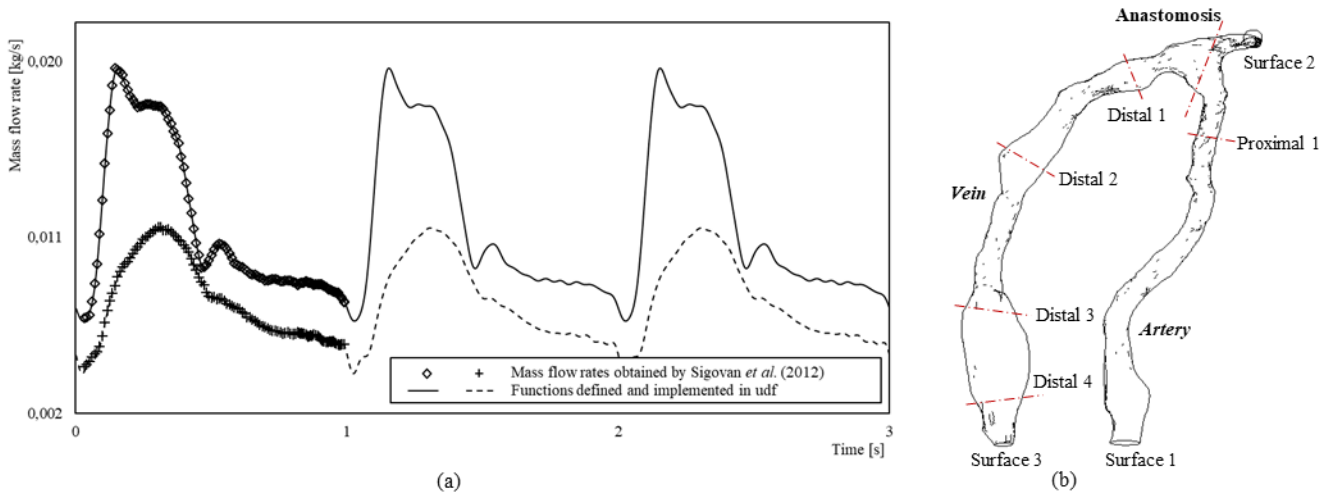

Figure 2. (a) Pulse of the mass flow rate and (b) Plans demarcated along the AVF.

3. RESULTS

3.1. Velocity field

The three-dimensional velocity field along the AVF corresponding to the maximum mass flow rate at t = 0.16 s at systole and t = 0.50 s at diastole is shown in Fig. (3). A well-defined primary flow pattern can be observed through the trajectory lines, with few disturbances along the artery, and showing maximum velocities of 1.30 m/s for t = 0.16 s and 0.70 m/s for t = 0,50 s. In the vein, the maximum velocities are 1.38 m/s for t = 0,16 s and 0.94 m/s for t = 0.50 s, located in the region immediately ascendant to the anastomosis with narrowing of the vessel diameter. Aside from the primary flow pattern, the presence of significant recirculations is observed in the vein, located mainly in the regions of anastomosis and the distal regions 1, 2, 3 and 4.

It can also be observed along the flow that velocity varies according to geometry, area of the cross-section, disturbances associated to recirculations in the axial and radial directions, in the regions of flow separation. Helical flows were also observed.

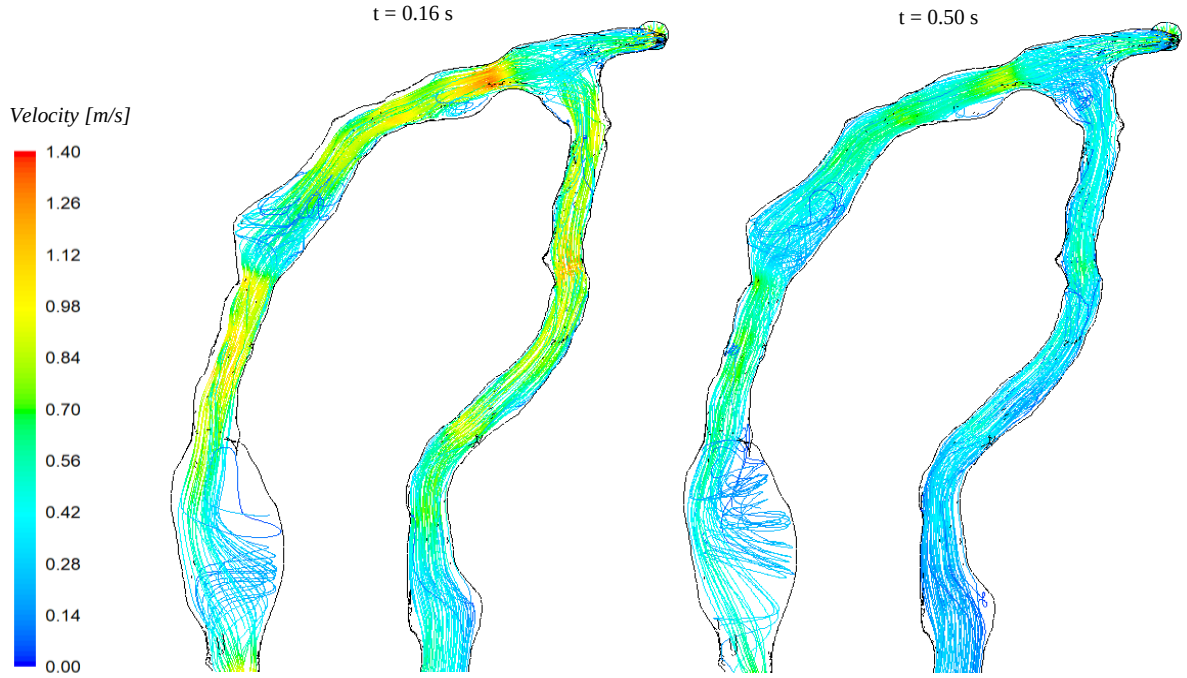

Figure 3. Trajectory lines along the flow in the AVF, for t = 0.16 s and for t = 0.50 s.

The presence of a small layer of clockwise helical flow is observed near the wall in the proximal plane 1, see Fig. (4a), for t = 0.16 s and for t = 0.50 s. The profile of velocity is consistent with what is expected for a laminar flow. The variation of magnitude in the velocity vectors was of 1.00 m/s maximum for t = 0.16 s and 0.50 m/s maximum for t = 0.50 s.

At the distal plane 1, immediately after the anastomosis, a primary flow pattern is observed in the superior right portion of its largest area, along with radial and axial recirculations and helical flow in the inferior portion. At t = 0.16 s, there are radial recirculations, the largest of which located in the inferior portion with clockwise orientation, along with a smaller recirculation oriented counterclockwise and located in the superior right portion of the plane, see Fig. (4b). The counterclockwise recirculation was not observed at t = 0.50 s. The variation in velocity was of 1.00 m/s maximum for t = 0.16 s and 0.70 m/s maximum for t = 0.50 s.

At the distal plane 2 (Fig. 4c), a primary flow pattern is observed in the superior right portion, as well as a helical flow located at nearly the entire periphery of the plane and radial recirculation. The area filled by the primary flow is decreasing when compared at t = 0.16 s and t = 0.50 s, being mostly occupied by radial recirculation and secondary helical flow. The variation of magnitude in the velocity vectors was of 0.60 m/s maximum for t = 0.16 s and 0.50 m/s maximum for t = 0.50 s.

At the distal plane 3 (Fig. 4d), a primary flow pattern located in the left side of the plane is observed, as well as a secondary helical flow and radial recirculations in the remaining area. It is noted that the secondary helical flow and the radial recirculations have velocity vectors with greater magnitudes at t = 0.50 s than at t = 0.16 s. The variation of magnitude in the velocity vectors was of 0.78 m/s maximum for t = 0.16 s and 0.60 m/s maximum for t = 0.50 s.

At the distal plane 4 (Fig. 4e), only a small area with primary flow pattern is observed, while the largest portion noticeably corresponds to that of secondary helical flow and radial recirculations. It is also noted that between the distal planes 3 and 4 there was a transformation of primary flow into secondary helical flow and radial recirculation, predominantly oriented clockwise to the plane. The variation of magnitude in the velocity vectors was of 0.40 m/s maximum for t = 0.16 s and 0.49 m/s maximum for t = 0.50 s.

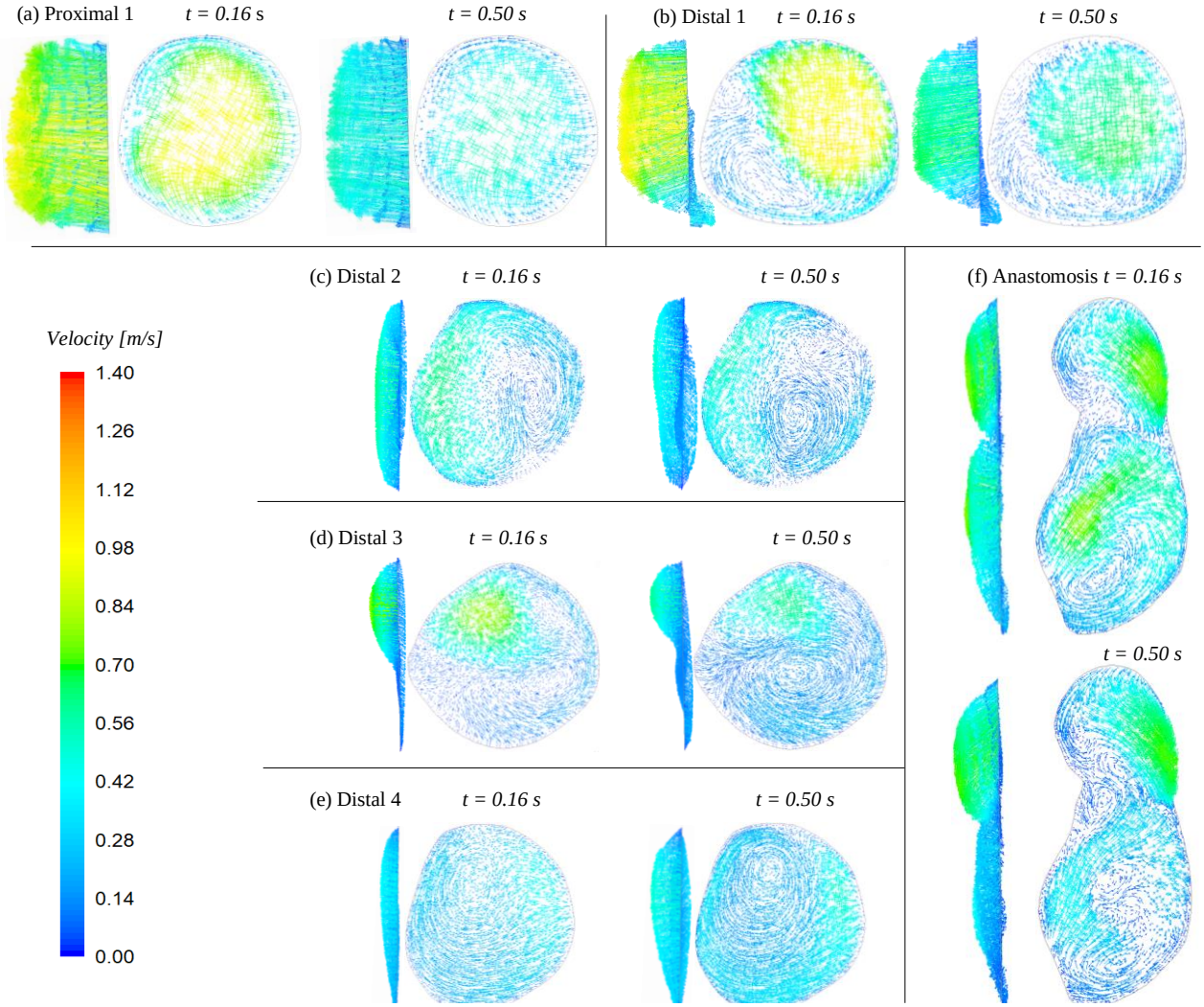

Figure 4. Vector planes for the planes studied along the flow in the AVF, for t = 0.16 s and for t = 0.50 s.

In the anastomosis (Fig. 4f), the meeting of two primary flow patterns is observed. Two recirculation regions are evidenced, in the left side in the sense of the arterial flow and in the left side propagating downwards in the sense of the venous flow, with greater intensity at t = 0.16 s and smaller intensity at t = 0.50 s. The variation of magnitude in the velocity vectors was of 0.78 m/s maximum for t = 0.16 s and 0.71 m/s maximum for t = 0.50 s.

3.2. Shear Stress

The distributions of the wall shear stress corresponding to the mass flow rate at t = 0.16 s at systole and for t = 0.50 s at diastole, along the AVF, are presented in Fig. (5). It was observed that along the AVF the wall shear stress presented no regularity, with values varying according to the cross section area and velocity. Higher stresses were noted at areas where there was narrowing of the vessel. In the artery, a maximum shear stress of 40 Pa was calculated at t = 0.16 s and of 15 Pa at t = 0.50 s. In the vein, a maximum wall shear stress of 49 Pa was calculated at t = 0.16 s and of 27 Pa at t = 0.50 s.

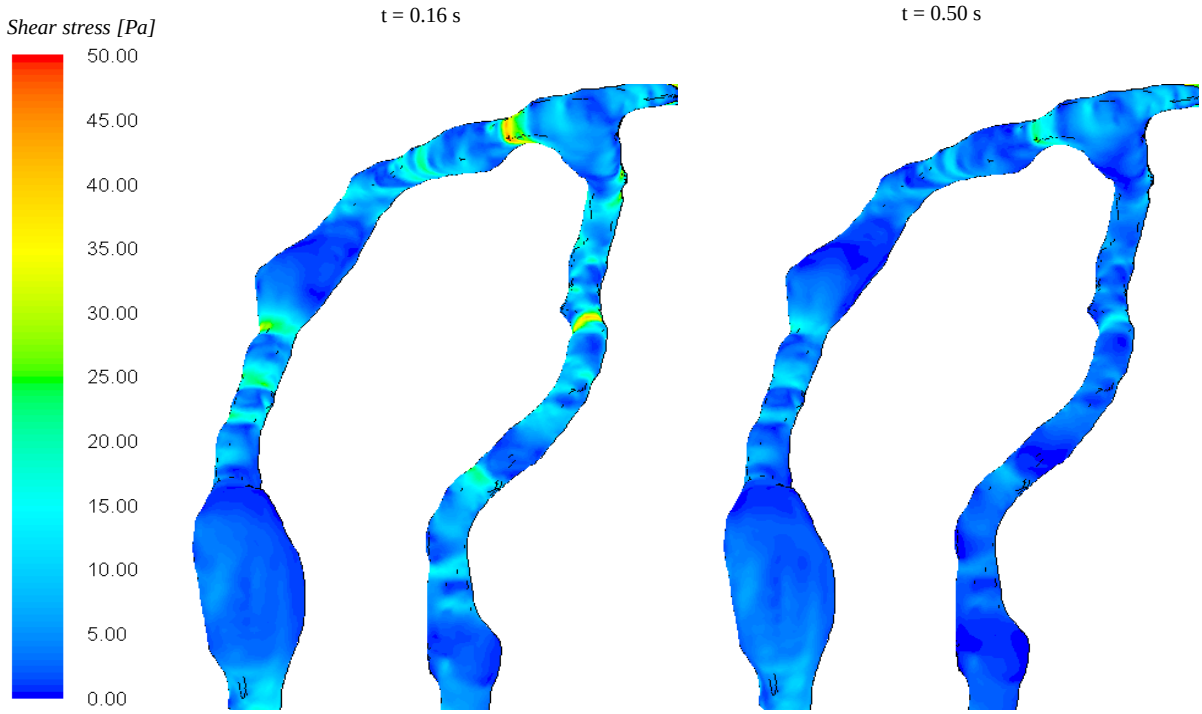

Figure 5. Distribution of wall shear stress along the AVF, at t = 0.16 s and at t = 0.50 s.

4. DISCUSSION

In this study, a detailed flow field along the AVF was obtained by means of numerical simulation. The geometrical model was obtained through a computed tomography scan. The assumptions made were of the blood as a Newtonian fluid, incompressible flow and pulsatile flow, with mass flow rate varying along the pulse.

According to the results for the flow field presented along the artery, before the anastomosis, the presence of disturbances along the flow was not noticed, as presented in Fig. (3). The flow tends towards a primary flow pattern with parabolic velocity profile, as expected of a laminar flow. However, there is a small distortion, which can be attributed to a lack of space for the velocity profile to develop, due to the changes in geometry. According to Sivanesan *et al.* (1999), when there are no recirculations, the blood formed elements occupy the central axial current, thus avoiding their sedimentation on the vessel wall.

In the anastomosis and distal regions, the presence of axial and radial recirculations was observed, as shown in Fig. (4bcdef). Bessa (2004) studied three types of *in vivo* surgical techniques for AVF and concluded that the recirculation and separation zones occurred for all techniques, especially in the anastomosis regions. This endorses the observation that the presence of the connection between artery and vein (anastomosis) as well as the variations in the geometry of the vessels cause disturbances in the primary flow, forming regions of recirculation with low wall shear stress, since the velocity in these regions is lower than in the primary flow. This characteristic was intensified in the distal regions at systole for t = 0,50 s, as shown in Fig. (4f). It is therefore possible to infer that the blood formed elements will be in recirculation for a larger amount of time, and thus may excessively collide with the endothelial wall.

As can be seen in Fig. (5), at the region where there is narrowing of the vessel immediately after the anastomosis, the values for wall shear stress reach 49 Pa. According to Fry (1968), shear stress ranging from 35 to 40 Pa can damage the

endothelial cells, leading to their denudation. For the scarring process, myointimal hyperplasia occurs, leading to obstruction of the vessel's cross section and causing loss of function of the AVF. Carroll *et al.* (2011) shows that myointimal hyperplasia occurs at regions of high wall shear stress.

It is worth noting that for the values observed in this study through numerical simulations, only the effects of the flow were considered as acting upon the vessel walls, though in actuality the oscillatory motion of the walls due to the pulsatile flow can have a remarkable effect on the flow's velocity field and wall shear stress. Thus, future studies analysing the solid-fluid and fluid-solid interactions will be necessary. Furthermore, according to Sigovan (2013) it is possible that high flow rates and stenotic constrictions may lead to transitional or turbulent flow in the AVF. Therefore, further studies will be needed to determine if the laminar flow model is truly the most appropriate.

5. CONCLUSION

According to the literature presented and the results obtained through this study, the detailed visualization of the flow field along the AVF has become essential to the advance of studies on the influence of hemodynamic factors on the vascular pathologies mentioned.

6. REFERENCES

BASSIOUNY, H.S. *et al*. Anastomotic intimal hyperplasia: mechanical injury or flow induced. **Journal of Vascular Surgery**, Chicago, v. 15, p. 708-716, 1992.

BESSA, K.L. Análise comparativa de fluxo em fístula arteriovenosa. 2004. 169 f. Dissertação (Mestrado em Engenharia Mecânica) – Escola Politécnica da Universidade de São Paulo, São Paulo, 2004.

BESSA, K.L.; ORTIZ, J.P. Flow visualization in arteriovenous fistula and aneurysm using computational fluid dynamics. **Journal of Visualization**, Tokyo, v. 12, p. 95-107, 2009.

CARROL, G.T. *et al.* Realistic temporal variations of shear stress modulate MMP-2 and MCP-1 expression in arteriovenous vascular access. **Cellular and Molecular Bioengineering**, New York, v. 2, p. 591-605, 2011.

CARROL, G.T. *et al.* Wall shear stresses remain elevated in mature arteriovenous fistulas: a case study. **Journal of Biomechanical Engineering**, New York, v. 133, 2011.

FRY, D.L. Acute vascular endotelial changes associated with increased blood velocity gradientes. **Circulation Research**, Baltimore, v. 22, p. 165-197, 1968.

GIDDENS, D. P.; ZARINS, C. K.; GLAGOV, S. The role of fluid mechanics in the localization and detection of atherosclerosis. **Journal of Biomechanical Engineering,** New York, v. 115, p. 588-594, 1993.

GILL, S. *et al.* Multi-disciplinary vascular access care and access outcomes in people starting hemodialysis therapy. **Clinical Journal of the American Society of Nephrology: CJASN**, Washington, v. 12, p. 1-9, 2017. Acesso em: 02 out. 2017. doi: 10.2215/CJN.03430317.

LINARDI, F. *et al.* Acesso vascular para hemodiálise: Avaliação do tipo e local anatômico em 23 unidades de diálise distribuídas em sete estados brasilieiros. **Revista do Colégio Brasileiro de Cirurgiões**, Rio de Janeiro, v. 30, p. 183-193, 2003.

LOK, C.E. Fistula First Initiative: Advantages and Pitfalls. **Clinical Journal of the American Society of Nephrology**, Washington, v. xxx, p. 1043-1053, 2017. Disponível em: <cjasn.asnjournals.org/content/2/5/1043.logn>. Acesso em: 02 out. 2017. doi: 10.2215/CJN.01080307.

PERRAULT, L.P. *et al.* Effects of the occlusion devices for minimally invasive coronary artery bypass surgery on coronary endothelial function of atherosclerosis arteries., **The Heart Surgery Forum**, Virginia, v. 3, p. 287-292, 2000.

RUBANYI, G.M. The role of endothelium in cardiovascular homeostasis. **Journal of cardiovascular pharmacology**, New York, v. 22, p. S1-S14, 1993.

SIGOVAN, M. *et al.* Vascular remodeling in autogenous arterio-venous fistulas by MRI and CFD. **Annals of Biomedical Engineering**, New York, v. 41, p. 657-668, 2013.

SIVANESAN, S.; HOW, T.V.; BAKRAN, A. Sites of stenosis in AV fistulae for haemodialysis access. **Nephrology, dialysis, transplantation: official publication of the European Dialysis and Transplant Assocciation – European Renal Association**, Oxford, v. 14, p. 118-120, 1999.

7. ACKNOWLEDGEMENTS

We thank the support of the Computational Fluid Dynamics Laboratory of the Federal University of Rio Grande do Norte.

8. RESPONSIBILITY FOR THE INFORMATION

The authors are solely responsible for the information included in this work.